ACS APPLIED BIO MATERIALS

www.acsabm.org Article

Near-Infrared Probes Designed with Hemicyanine Fluorophores Featuring Rhodamine and 1,8-Naphthalic Derivatives for Viscosity and HSA Detection in Live Cells

Adenike Mary Olowolagba, Omowunmi Rebecca Aworinde, Sushil K. Dwivedi,* Micah Olamide Idowu, Dilka Liyana Arachchige, Crystal Wang, Olivya Rose Graham, Joseph Peters, Grace Rickauer, Thomas Werner, Athar Ata,* Rudy Lin Luck,* and Haiying Liu*

Cite This: https://doi.org/10.1021/acsabm.4c01721 Read Online

ACCESS | Metrics & More | Article Recommendations | Supporting Information

ABSTRACT: This paper presents the development of near-infrared (NIR) fluorescent probes, **A** and **B**, engineered from hemicyanine dyes with 1,8-naphthalic and rhodamine derivatives for optimized photophysical properties and precise mitochondrial targeting. Probes **A** and **B** exhibit absorption peaks at 737 nm and low fluorescence in phosphate-buffered saline (PBS) buffer. Notably, their fluorescence intensities, peaking at 684 (**A**) and 702 nm (**B**), increase significantly with viscosity, as demonstrated through glycerol-to-PBS ratio experiments. This increase is attributed to restricted rotational freedom in the fluorophore and its linkages to rhodamine or 1,8-naphthalic groups. Theoretical modeling suggests nonplanar configurations for both probes, with primary absorptions in the rhodamine and hemicyanine cores (**A**: 543; **B**: 536 nm), and additional transitions to 1,8-naphthalic (**A**: 478 nm) and rhodamine (**B**: 626 nm) groups. Probe **A** is also responsive to human serum albumin (HSA), a key biomarker, with fluorescence increasing in HeLa cells as HSA concentrations rise. In contrast, probe **B** shows no response to HSA, likely due to steric hindrance from its bulky rhodamine group, illustrating a selectivity difference between the probes. Probe **B**, however, excels in mitochondrial imaging, confirmed through cellular and in vivo studies. In HeLa cells, it tracked viscosity changes following treatment with monensin, nystatin, and lipopolysaccharide (LPS), with fluorescence increasing in a dose-dependent manner. In fruit flies, probe **B** effectively detected monensin-induced viscosity changes, demonstrating its stability and *in vivo* applicability. These findings highlight the versatility and sensitivity of probes **A** and **B** as tools in biological research, with potential applications in monitoring mitochondrial health, detecting biomarkers like HSA, and investigating mitochondrial dynamics in disease.

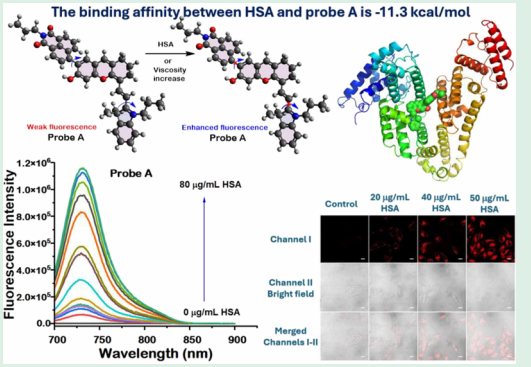

KEYWORDS: *viscosity, hemicyanine dye, rhodamine, 1,8-naphthalic derivative, near-infrared imaging, HSA, fluorescent probes*

INTRODUCTION

Mitochondria, the organelles responsible for cellular energy production, are indispensable for cellular metabolism, energy production, and regulation of apoptosis. These organelles convert nutrients into adenosine triphosphate (ATP) through oxidative phosphorylation and play vital roles in generating reactive oxygen species (ROS), calcium signaling, and regulating cell death pathways.[1−9] Given their central role, mitochondrial dysfunction is implicated in various illnesses, encompassing neurodegenerative diseases, cancer, and metabolic syndromes.[1−9] Consequently, understanding mitochondrial dynamics and properties in live cells is essential for both basic research and clinical applications.[1−9] Fluorescence microscopy has gained recognition as an effective tool for real-time observation of intracellular processes. Near-infrared (NIR) fluorescent probes offer significant advantages, such as reduced phototoxicity, enhanced tissue penetration, and minimal autofluorescence, making them ideal for live-cell imaging. Developing NIR probes that specifically target subcellular compartments like mitochondria enables detailed visualization and quantification of mitochondrial dynamics and functions.[10−16] Hemicyanine dyes have recently gained attention as promising candidates for NIR fluorescent probes due to their large quantum yields and wide Stokes shifts, tunable absorption and emission wavelengths, and excellent photostability and biocompatibility.[17−35] Such characteristics render them ideal for live-cell imaging and for creating probes

Received: November 18, 2024
Revised: December 25, 2024
Accepted: December 26, 2024

Scheme 1. NIR Fluorescent probes Derived from Hemicyanine Dyes Featuring Rhodamine and 1,8-Naphthalic Derivatives for Viscosity and HSA Detection

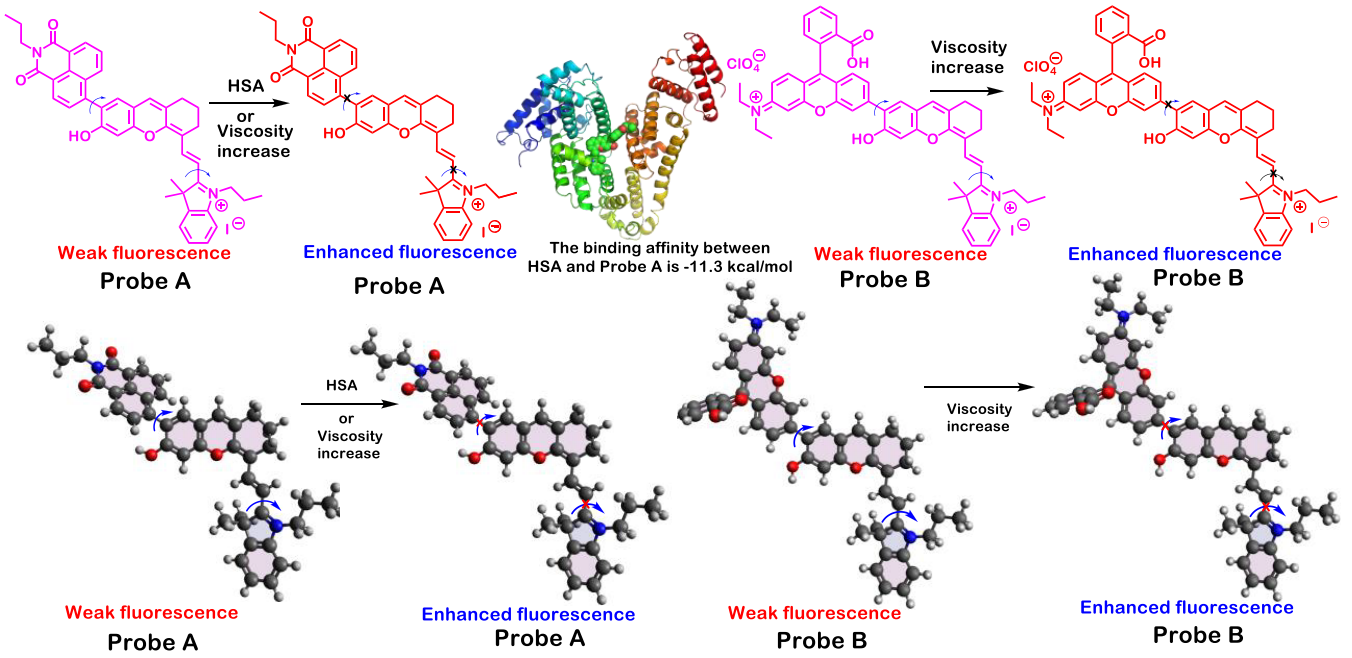

optimized for a range of biological uses.[17−19] An essential aspect of mitochondrial health that can be assessed with these probes is mitochondrial viscosity. Viscosity within mitochondria reflects their physical state and functionality, impacting processes such as oxidative phosphorylation and permeability transitions. It is also closely linked to the respiratory and metabolic states within the organelle, with deviations in viscosity often observed in pathologies such as neurodegenerative diseases, diabetes, and atherosclerosis.

Beyond mitochondrial function, monitoring human serum albumin (HSA) levels in cells provides critical insights into systemic health. HSA, one of the most abundant proteins in the body, is vital for maintaining osmotic pressure, balancing nutrition, and transporting a wide range of drugs and metabolites. Normal HSA concentrations in blood serum range from 35 to 50 g/L, while levels in urine remain below 30 mg/L in healthy individuals due to kidney filtration. Abnormal HSA levels serve as reliable indicators of liver and kidney function, with elevated levels in urine (albuminuria) often signaling early kidney impairment, and reduced blood levels (hypoproteinemia) commonly linked to liver diseases such as cirrhosis and chronic hepatitis.[36] Consequently, there is a growing need for rapid, specific, and cost-effective tools to monitor HSA levels in body fluids, as fluctuations in HSA can reflect early stages of disease and guide preventive care. Therefore, developing multifunctional NIR probes that can simultaneously monitor mitochondrial viscosity and HSA levels in live cells would offer a significant advancement in the real-time assessment of cellular and mitochondrial health. Such probes could serve as invaluable tools for disease diagnosis, treatment evaluation, and clinical applications, paving the way for more comprehensive insights into mitochondrial and systemic functions.[27−34,37−51]

In this manuscript, we describe the creation of innovative near-infrared (NIR) fluorescent probes, named probes **A** and **B**, which are derived from hemicyanine dyes with 1,8-naphthalic and rhodamine derivatives (Scheme 1). These probes were designed to enhance photophysical properties, including sensitivity to environmental factors such as viscosity, and to facilitate targeted cellular imaging. Probes **A** and **B** feature distinct absorption peaks at 684 and 741 nm, and 685 and 737 nm, respectively, and show minimal fluorescence in phosphate-buffered saline (PBS) buffer. Notably, their fluorescence intensity increases significantly with rising viscosity, demonstrated by modulating glycerol-to-PBS ratios in solution. This behavior is attributed to the restricted rotational freedom within the hemicyanine fluorophore and the constrained linkages between hemicyanine and 1,8-naphthalic or rhodamine groups, underscoring the probes' sensitivity to microenvironmental viscosity. To expand their potential applications, we investigated probes **A** and **B** for their ability to detect human serum albumin (HSA), a protein vital for numerous physiological functions and an important marker for assessing liver and kidney health. Probe **A** displayed a progressive increase in fluorescence intensity at 731 nm with increasing HSA concentrations in PBS buffer (pH 7.4) under 680 nm excitation, highlighting its high sensitivity to HSA and suggesting its potential for real-time HSA monitoring in biological systems. The binding affinity between HSA and Probe **A**, as determined through molecular docking, is -11.3 kcal/mol. In contrast, probe **B** exhibited no fluorescence response within this concentration range, likely due to steric hindrance from its bulky rhodamine residue, which may impede effective hydrophobic interactions with HSA. Beyond HSA detection, probe **B** was applied in cellular and *in vivo* imaging to evaluate its effectiveness in sensing viscosity changes. In HeLa cells, probe **B** successfully detected viscosity changes induced by treatments with monensin, nystatin, and bacterial lipopolysaccharide (LPS). Monensin, known to disrupt ion gradients, induced a dose-dependent increase in fluorescence, signifying increased cellular viscosity. Similarly, nystatin and LPS treatments resulted in enhanced fluorescence, consistent with elevated viscosity. Probe **B** also demonstrated strong performance in live fruit fly models, where monensin

https://doi.org/10.1021/acsabm.4c01721
ACS Appl. Bio Mater. XXXX, XXX, XXX−XXX

Scheme 2. Strategic Synthetic Route to Prepare Hemicyanine Dyes Featuring Rhodamine and 1,8-Naphthalic Derivatives for Mitochondrial Viscosity Detection (probes A and B)

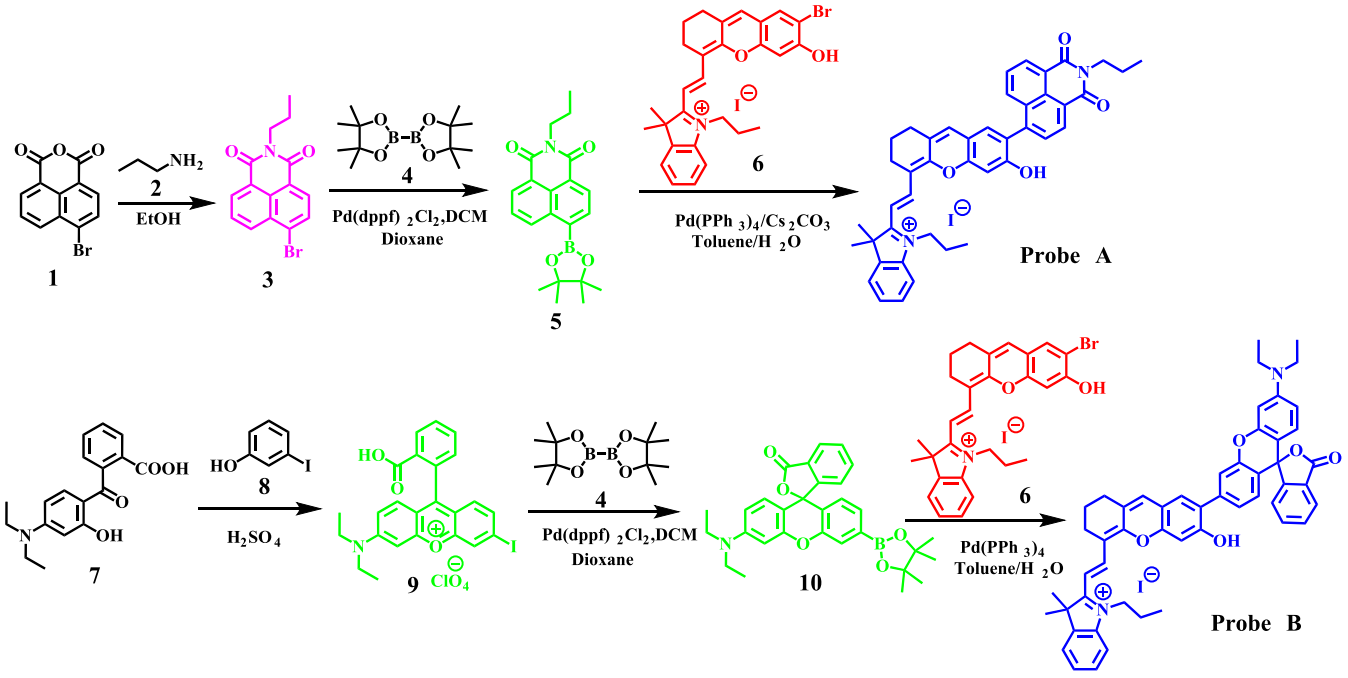

treatment correlated with a measurable increase in fluorescence intensity, further validating probe **B**'s utility for *in vivo* applications. Additionally, probe **A** was tested for HSA detection in live cell contexts. Overall, probe **B** represents a significant advancement in studying mitochondrial viscosity and cellular dynamics. Its high selectivity, excellent photostability, and low cytotoxicity make it a valuable tool for investigating mitochondrial function and stress responses across cell culture and live organisms. This work highlights the potential of probes **A** and **B** for expanding our understanding of mitochondrial biology and their promising biomedical applications.

EXPERIMENTAL SECTIONS

Synthesis of probes A and B. *Synthesis of probe A.* ^{1}H NMR (500 MHz, $CDCl_3$), δ (ppm): 1.02 (3H, t, J = 7.5 Hz), 1.07 (3H, t, J = 7.5 Hz), 1.74 (6H, s), 1.78 (2H, m), 1.87 (2H, m), 1.95 (2H, t, J = 5.0 Hz), 2.66 (2H, t, J = 5.0 Hz), 2.77 (2H, t, J = 7.5 Hz), 3.85 (2H, t, J = 7.5 Hz), 4.17 (2H, t, J = 7.5 Hz), 5.76 (1H, d, J = 10.0 Hz), 6.92 (1H, d, J = 10.0 Hz), 7.12 (3H, m), 7.39 (1H, s), 7.63 (1H, t, J = 7.5 Hz), 7.73 (1H, d, J = 10.0 Hz), 8.16 (1H, d, J = 10.0 Hz), 8.24 (1H, d, J = 15.0 Hz), 8.59 (1H, d, J = 5.0 Hz), 8.63 (1H, d, J = 5.0 Hz). ^{13}C NMR (125 MHz, $CDCl_3$) δ (ppm): 11.12, 11.53, 11.55, 11.74, 20.31, 20.33, 21.23, 21.41, 21.43, 24.47, 24.49, 28.21, 28.67, 41.84, 45.07, 48.06, 48.10, 99.99, 104.24, 104.28, 108.66, 108.74, 115.53, 115.66, 121.81, 122.24, 122.60, 126.38, 128.22, 128.27,128.43, 128.50, 130.50, 130.51, 130.69, 130.90, 131.02, 133.52, 133.55, 139.69, 144.27, 164.31, 164.47, 164.49. LCMS m/z = 649.50, calculated m/z = 649.31.

Synthesis of probe B. ^{1}H NMR (500 MHz, $CDCl_3$), δ (ppm): 1.0 (3H, t, J = 7.5 Hz), 1.15 (6H, t, J = 7.5 Hz), 1.70 (6H, s), 1.76 (2H, m), 1.86 (2H, t, J = 7.5 Hz), 2.56 (2H, t, J = 5.0 Hz), 2.70 (2H, t, J = 5.0 Hz), 3.29 (4H, t, J = 7.5 Hz), 3.73 (2H, t, J = 7.5 Hz), 5.79 (1H, d, J = 10.0 Hz), 6.36 (2H, d, J = 10.0 Hz), 6.59 (1H, d, J = 10.0 Hz), 6.74 (1H, d, J = 10.0 Hz), 6.90 (1H, d, J = 5.0 Hz), 7.13 (1H, t, J = 7.5 Hz), 7.19 (1H, d, J = 10.0 Hz), 7.29 (4H, m), 7.38 (1H, s), 7.59 (4H, m), 8.01 (1H, d, J = 10.0 Hz), 8.18 (1H, d, J = 10.0 Hz). ^{13}C NMR (125 MHz, $CDCl_3$) δ (ppm): 11.62, 12.52, 12.55, 12.57, 20.36, 24.14, 24.49, 28.29, 28.52, 44.42, 44.45, 63.41, 84.24, 97.55, 104.26, 105.06, 108.20, 117.55, 117.57, 117.68, 122.34, 122.37, 124.30, 124.31, 124.74, 126.98, 127.47, 127.49, 128.23, 128.24, 128.67, 128.89, 128.90, 129.49, 134.90, 149.56, 151.30, 152.93, 153.25, 169.70. LCMS m/z = 781.50, calculated m/z = 781.36.

RESULTS AND DISCUSSION

Probe Synthetic Strategy. Hemicyanine dyes are renowned for their exceptional photostability and biocompatibility, attributes that make them particularly well-suited for live-cell imaging applications. Their photophysical properties, including tunable absorption and emission wavelengths, can be finely adjusted to optimize performance for various biological applications.[17−34] To further enhance their sensitivity to viscosity changes, we designed and synthesized hemicyanine dyes incorporating 1,8-naphthalic and rhodamine moieties through a Suzuki-palladium-catalyzed reaction, aiming to create probes with improved viscosity sensitivity (probes **A** and **B**) (Scheme 2). The construction of probe **A** involved the introduction of an *N*-propyl-1,8-naphthalimide moiety into a hemicyanine dye. This was achieved through a two-step Suzuki-palladium-catalyzed process. Initially, we prepared 4-(4,4,5,5-tetramethyl-1,3,2-dioxaborolan-2-yl)-*N*-propyl-1,8-naphthalimide (**5**) by coupling 4-bromo-*N*-propyl-1,8-naphthalimide (**3**) with bis(pinacolato)diboron. This intermediate served as a key component for the subsequent reaction. In the second step, intermediate **5** was coupled with a bromo-functionalized hemicyanine dye (**6**) using the Suzuki-palladium-catalyzed reaction, resulting in probe **A**. This probe features a hemicyanine dye with an *N*-propyl-1,8-naphthalimide residue, designed to respond to changes in viscosity by altering its photophysical properties. Similarly, probe **B** was synthesized by incorporating a rhodamine moiety into the hemicyanine dye structure. We first synthesized 3′-(diethylamino)-6′-(4,4,5,5-tetramethyl-1,3,2-dioxaborolan-2-yl)-spiro[isobenzofuran-1(3H),9′-[9*H*]xanthen]-3-one (**10**) through a Suzuki-palladium-catalyzed coupling reaction of 3′-(diethylamino)-6′-iodospiro[isobenzofuran-1(3H),9′-[9*H*]-

https://doi.org/10.1021/acsabm.4c01721
ACS Appl. Bio Mater. XXXX, XXX, XXX−XXX

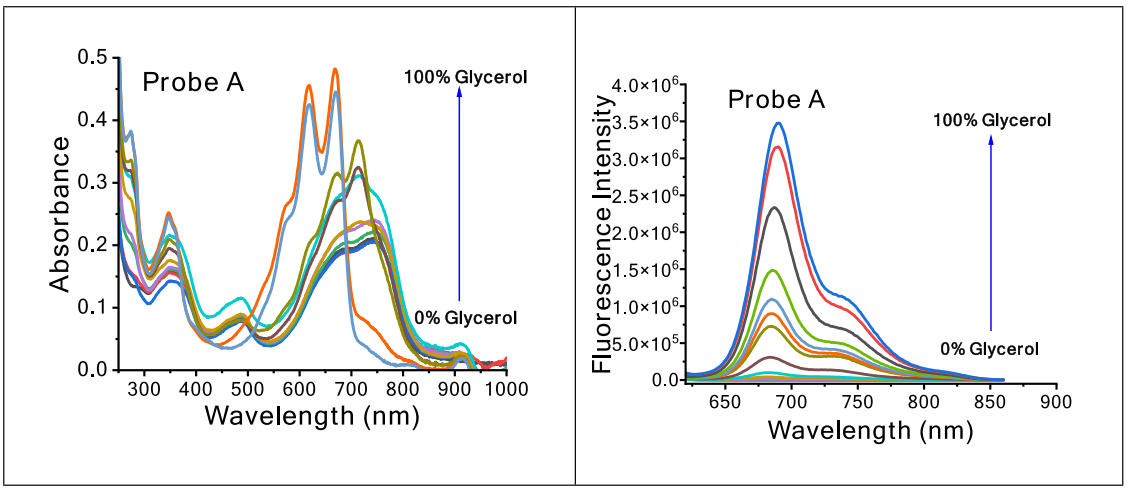

Figure 1. Absorbance (left) and emission (right) profiles of 10 μM probe **A** in mixture containing pH 7.4 PBS buffer and glycerol in different proportions, captured with 600 nm excitation.

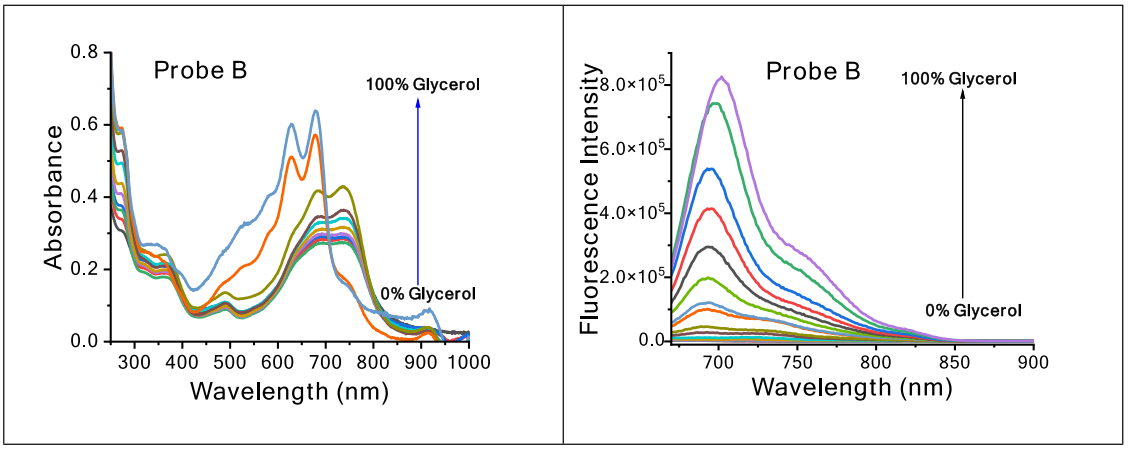

Figure 2. Absorbance (left) and emission (right) profiles of 10 μM probe **B** in solutions containing pH 7.4 PBS buffer and glycerol in different proportions, captured with 600 nm excitation.

xanthen]-3-one (**9**) with bis(pinacolato)diboron (Scheme 2). This intermediate was then reacted with a bromo-functionalized hemicyanine dye (**6**) via another Suzuki-palladium-catalyzed reaction, yielding probe **B** (Scheme 2). This probe incorporates a rhodamine moiety, designed to provide sensitivity to changes in viscosity by modulating its fluorescence properties. All intermediate and final probes were rigorously studied using nuclear magnetic resonance (NMR) and mass spectral analysis (Figures S1−S11). NMR spectra confirmed the molecular structures and purity of the intermediates and probes (Figures S1−S5 and S7−S10). Mass spectrometry provided additional verification of molecular weights and the integrity of the synthesized compounds (Figures S6 and S11). These probes were designed to enhance the sensitivity of hemicyanine dyes to viscosity changes, making them suitable for detailed studies of mitochondrial viscosity in live cells (Figures S12). The introduction of specific moieties through well-established synthetic methods ensures that the probes have optimized photophysical properties for precise and reliable measurement of viscosity changes, contributing valuable insights into mitochondrial dynamics and function.

Probe Optical Sensing of Viscosity. To evaluate the fluorescence responsiveness of probes **A** and **B** to viscosity alterations, a series of experiments were performed using PBS buffer mixed with varying glycerol concentrations. Probes **A** and **B** were prepared at a 10 μM concentration in PBS buffer (pH 7.4). The viscosity of the solutions was systematically adjusted by incorporating glycerol in proportions ranging from 0 to 100%. In only PBS buffer, the probes displayed broad absorption peaks featuring two maxima, probes **A** (684, 741 nm) and **B** (685, 737 nm) (Figures 1 and 2). Under these solvent conditions, probes **A** and **B** exhibited minimal fluorescence, with weak emissions observed at 682 and 692 nm, respectively (Figures 1 and 2), As the glycerol concentration increased, notable shifts in absorbance and enhancements in fluorescence intensities were observed for both probes (Figures 1 and 2). A strong linear relationship is observed between log (I_{max}) and log (η) for probes **A** and **B**, with correlation coefficients of 0.9870 and 0.9857, respectively (Figure S12). This relationship supports their use for the quantitative determination of viscosity. The absorbance spectrum in 100% glycerol, probe **A** featured two peaks at 619 and 671 nm and probe **B** contained two defined peaks at 629 and 680 nm (Figure 1). Under these conditions, probe **A** exhibited a marked increase in fluorescence emission at 690 nm (740 nm, shoulder), while probe **B** demonstrated similar enhancement at 702 nm (747 nm, shoulder) (Figure 2). This

https://doi.org/10.1021/acsabm.4c01721
ACS Appl. Bio Mater. XXXX, XXX, XXX−XXX

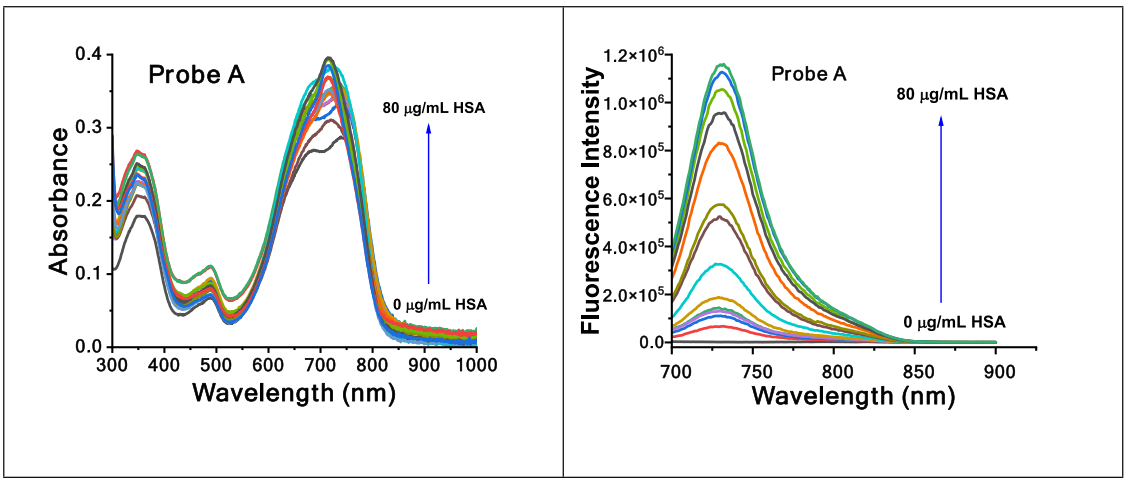

Figure 3. Absorbance (left) and emission (right) profiles of 10 μM probe **A** with and without different HSA concentrations in pH 7.4 phosphate buffers using 680 nm excitation.

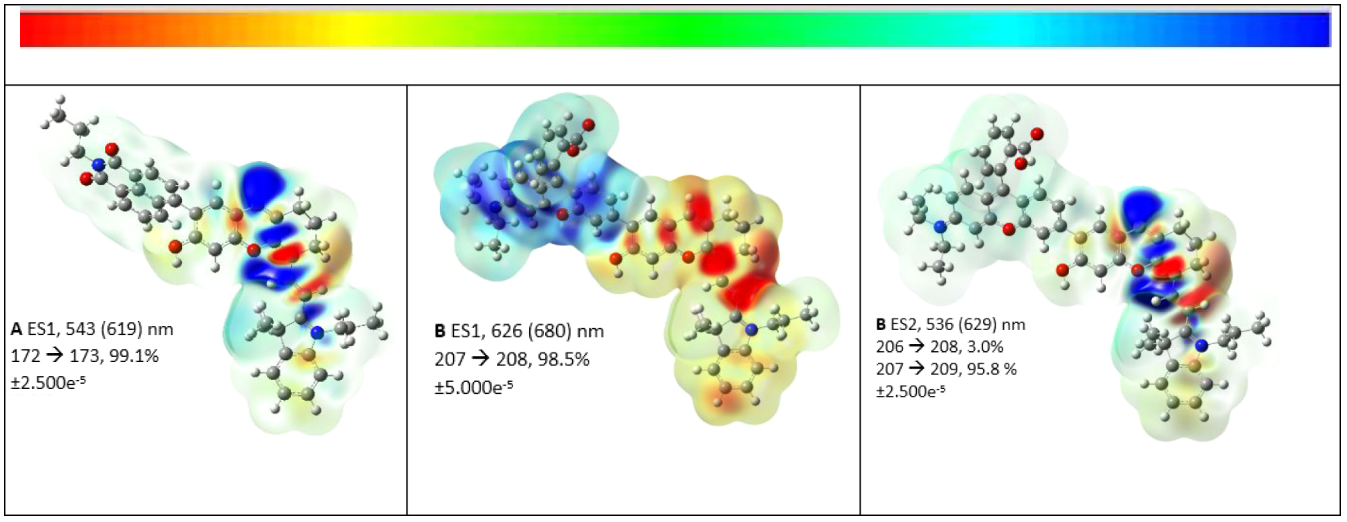

Figure 4. Schematic representations of disparities in current density for electronic transitions are illustrated as isosurfaces for probe **A** (left) and probe **B** (ES1, middle, ES2, right). The quantity of energized states (ES), including both the theoretically predicted and empirically determined wavelengths, as well as the transitions, are outlined along with their relative contribution values. The values related to the color grading at the top of the figure are also specified. To provide additional clarity, diagrams of the LCMOs marked with numerical identifiers are included in the Supporting Information.

shift in absorbance in the probes is attributed to aggregation effects in water with the broad peak and to isolated molecules in 100% glycerol, resulting in sharper better-defined absorbances. It is known that aggregation quenches fluorescence,[52] thus in the buffer solution, the probes do not emit much. However, the enhancement in fluorescence could be attributed to the increased viscosity, which restricts the rotational freedom of the carbon−carbon bond connections between the hemicyanine fluorophore and the rhodamine or 1,8-naphthalic moieties. This restriction reduces nonradiative decay pathways and leads to increased fluorescence emissions. The data confirms that both probes **A** and **B** are highly sensitive to viscosity changes (Figures 1 and 2). Their fluorescence response to varying glycerol concentrations provides a reliable and measurable indicator of viscosity (Figure S12). This high sensitivity underscores the potential of these probes for applications in monitoring viscosity-related phenomena in biological systems. The capability to detect real-time viscosity changes makes probes **A** and **B** crucial aids in studying mitochondrial viscosity and other cellular processes where viscosity plays a critical role.

We further evaluated the ability of probes **A** and **B** to determine human serum albumin (HSA). Probe **A** presents a broad near-infrared absorption peak at 715 nm, a visible absorption peak at 352 nm, and a weak near-infrared fluorescence peak at 731 nm in the absence of HSA (Figure 3). Upon gradually increasing HSA concentrations from 0 μM to 80 μM in PBS buffer (pH 7.4), the emission intensity of probe **A** at 731 nm increases progressively with linear response up to 80 μM under 680 nm excitation (Figures 3 and S13). In contrast, probe **B** does not exhibit any fluorescence response to HSA within the same concentration range. This lack of response is likely due to the bulky rhodamine residue in probe **B**, which may hinder effective hydrophobic interactions with HSA.

Theoretical Calculations. The procedures for carrying out these calculations are outlined in the Supporting Information and adhere to the methods described earlier.[53,54] Probe **A** is

https://doi.org/10.1021/acsabm.4c01721
ACS Appl. Bio Mater. XXXX, XXX, XXX−XXX

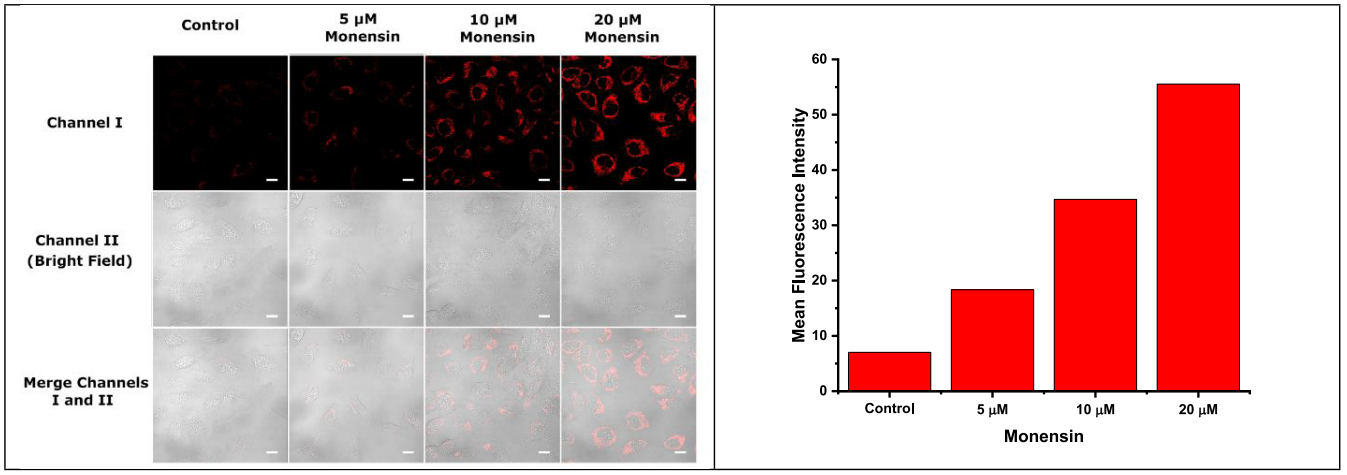

Figure 5. Fluorescence images of HeLa cells exposed to increasing concentrations of Monensin (from 0 to 20 μM) for a duration of 30 min, Afterward, the cells were under exposure to probe **B** (5 μM) in Dulbecco's modified eagle medium (DMEM) for 20 min. Fluorescence was detected in the 680−780 nm range, using a 630 nm excitation. The scale bar is equivalent to 50 μm.

constituted of three sections, the central rhodamine section linked on the end to a 1,8-naphthalic derivative (i.e., 2-propyl-1*H*-benzo[de]isoquinoline-1,3(2*H*)-dione) with an interplanar twist of 64.1° and at the other end coplanar with a dimethyl hemicyanine (Figure S20). In contrast, probe **B** consists of coplanar central rhodamine and hemicyanine sections but a more complex rhodamine (3′-(diethylamino)-3*H*-spiro-[isobenzofuran-1,9′-xanthen]-3-one) is attached at the other end at an interplanar angle of 44.0° (Figure S23).

Current density illustrations for the lowest energy calculated absorptions for the probes are detailed in Figure 4. Interestingly, the calculated absorption spectrum for probe **A**, Figure S21 consisted in part of a broad absorption at 543 nm with a very weak peak at 478 nm. The representation of the current density in Figure 4 together with the LCAOs for the transition (Figure S22) suggests that the main absorption is due to the movement of electron density essentially localized on the central rhodamine and the dimethyl hemicyanine moieties. The much weaker transition was due to a transfer of electron density from the rhodamine and dimethyl hemicyanine section to the 1,8-naphthalic derivative which, because these groups were not planar, resulted in the very weak oscillation factor of 0.0079, Table S2 and Figure S22.

By contrast, probe **B** consisted of a broad peak at 536 nm with a shoulder peak at 626 nm. The shoulder peak is due to the transfer of electron density from the coplanar regions consisting of the central rhodamine and the dimethyl hemicyanine moieties to the more complex rhodamine on the left of the illustration, Figures 4 and S24. The nature of the electronic transition of the broad peak at 536 is similar in flow to that for probe **A** described above suggesting that increasing viscosity may result in less rotation around the C−C atom single bond linkage with the central group and the entities to the left of both probes resulting in a more efficient transfer of electron density and increased fluorescence as displayed in Figures 1 and 2. The molecular docking analysis reveals a binding affinity of -11.3 kcal.mol between HSA and Probe **A** (Table S5 and Figures S26-S34).

Probe Selectivity, Photostability, pH Effect, and Cytotoxicity. The high selectivity of the probes toward viscosity was rigorously tested against a wide array of common interfering substances, including cations, anions, amino acids, and biothiols. In a pH 7.4 PBS buffer, the emission intensity of probe **A** (10 μM) was measured upon excitation at 600 nm, while probe **B** (10 μM) was measured upon excitation at 650 nm. Probes **A** and **B** exhibit extremely weak emission at 786 and 788 nm, accordingly, and maintain stability without sensitivity to pH changes between 5.7 and 8.5 in PBS buffers (Figure S18). The selectivity assessment involved introducing various potentially interfering species at a concentration of 100 μM. These species included anions (SO_3^{2-}, HCO_3^{2-}, NO_3^-, CN^-, Cl^-), cations (Mg^{2+}, Fe^{2+}, Co^{2+}, Na^+, K^+), biothiols (glutathione (GSH)) and amino acids (DL-valine, methionine (Met), L-cysteine (Cys), DL-lysine). The results demonstrated that both probes **A** and **B** maintained a significant fluorescence response to viscosity changes with minimal interference from these substances (Figure S14). Additionally, glycerol (100% concentration) was used as a viscosity control to confirm the probes' sensitivity to viscosity. These findings highlight the exceptional selectivity of probes **A** and **B**, making them well-suited for monitoring viscosity-related phenomena in biological systems. Similarly, probe **A** was tested to assess its selectivity for HSA in the presence of the corresponding ions (Figure S15).

The photostability of the probes was evaluated to evaluate their resilience under continuous light exposure, a critical attribute for reliable long-term imaging applications. Both probes were dissolved in glycerol solution at a concentration of 10 μM. The emission intensity of probe **A** was measured upon excitation at 600 nm, and probe **B** at 650 nm. The results, depicted in Figure S16, illustrate that both probes maintained 95% of their initial fluorescence intensity even after 2 h of continuous excitation. This high level of photostability ensures that probes **A** and **B** can deliver stable and accurate fluorescence signals during extended imaging sessions, making them exceptionally suitable for monitoring dynamic biological processes where prolonged light exposure is necessary. The robust photostability further underscores the utility of these probes in real-time, live-cell imaging applications, facilitating the investigation of viscosity-related changes in biological systems with minimal photobleaching concerns.

The cytotoxicity of probe **B** was quantified with the (3-[4,5-dimethylthiazol-2-yl]-2,5 diphenyl tetrazolium bromide) (MTT) assay to ensure their biocompatibility for live-cell

https://doi.org/10.1021/acsabm.4c01721
ACS Appl. Bio Mater. XXXX, XXX, XXX−XXX

imaging applications.[8,22,55−63] HeLa cells were subjected to varying probe concentrations, with a particular focus on the 50 μM concentration (Figure S17). The cell viability was determined after 24 h of incubation. The analysis confirmed that more than 87% of HeLa cells remained viable at a 50 μM concentration of probe **B**, indicating low cytotoxicity. This high level of cell viability confirms that probe **B** is well-tolerated by live cells, making them suitable for long-term studies without compromising cell health. These findings support the potential of these probes for use in dynamic biological environments, where maintaining cell viability is crucial for accurate and reliable imaging. The MTT assay analysis underscores biological compatibility of probe **B**, further validating their application in live-cell imaging to monitor viscosity-related changes and other cellular processes.

Cellular Fluorescence of HeLa Cells. Monensin acts as an ionophore, disrupting ion gradients across cellular membranes by facilitating the transport of sodium (Na^+) and potassium (K^+) ions.[64] This disruption leads to an imbalance in ion homeostasis, causing cellular stress and changes in the cytoplasmic environment.[64] One cellular response to this stress is an increase in intracellular viscosity, attributed to macromolecular aggregation, cytoskeletal reorganization, and altered organelle dynamics.[30,65] In this study, HeLa cells were exposed to monensin at concentrations of 0, 5, 10, and 20 μM (with 0 μM as control) in cell culture media for 30 min to induce changes in cellular viscosity. Following monensin treatment, the cells were cultured with probe **B** (5 μM) in growth medium for an additional 20 min to ensure sufficient probe uptake and fluorescence response. Images were recorded through fluorescence microscopy within the 680 to 780 nm wavelength range using a 630 nm excitation source to monitor fluorescence changes in response to different levels of monensin-induced viscosity variations (Figure 5). The fluorescence microscopy images revealed a substantial elevation of cellular fluorescence intensity when the monensin concentration increased (Figure 5). In the control sample (0 μM monensin), minimal fluorescence was observed, indicating a baseline viscosity with probe **B**. At 5 μM monensin, a noticeable increase in fluorescence was detected, suggesting a moderate rise in cellular viscosity. With 10 μM monensin, there was a further increase in fluorescence intensity, correlating with a more significant viscosity enhancement. The highest fluorescence intensity was observed at 20 μM monensin, indicating a substantial increase in cellular viscosity. The increased fluorescence intensity of probe **B** with rising monensin concentrations demonstrates the probe's effectiveness in sensing these viscosity changes (Figure 5). Probe **B**'s fluorescence mechanism relies on its unique molecular structure, which includes a hemicyanine fluorophore and a rhodamine fluorophore linked by a single bond. As viscosity increases, the restricted rotational freedom of these single bonds within the hemicyanine and at the hemicyanine-rhodamine junction reduces nonfluorescent relaxation pathways, leading to enhanced fluorescence emission. This restriction reduces nonradiative decay pathways, resulting in enhanced fluorescence emissions. This property makes probe **B** an excellent tool for detecting and monitoring viscosity changes within live cells. The ability to monitor such changes provides valuable insights into cellular processes and conditions where viscosity plays a crucial role, such as drug interactions, disease states, and metabolic activities.

To evaluate our hypothesis that probes **A** and **B** selectively target mitochondria because of their positive charge, which promotes electrostatic attraction to the negative charge across the mitochondrial membrane, we performed colocalization imaging studies. In these experiments, HeLa cells were pretreated with 5 μM Nystatin for 30 min to influence cellular conditions, subsequently incubated with either probe **A** (Figure S19) or probe **B**, along with the mitochondrial-selective dye MitoView 405. The findings revealed a considerable overlap between probe **B** and MitoView 405, yielding a high Pearson correlation coefficient of 0.966 (Figure 6). This high degree of colocalization confirms that probe **B** is

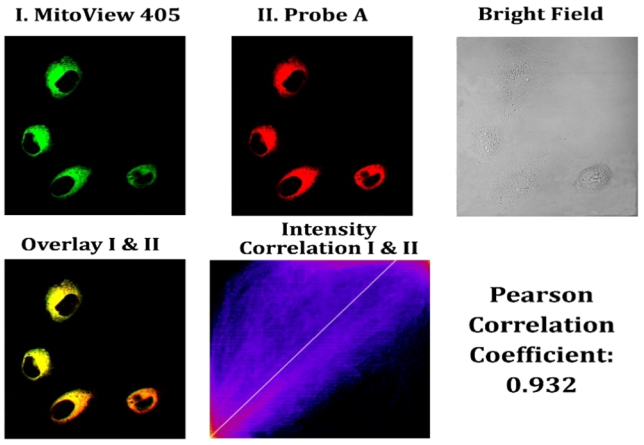

Figure 6. Emission images of HeLa cells with a 30 min treatment with 5 μM Nystatin, followed by a 20 min stimulation with 5 μM probe **B** and 5 μM MitoView 405. The blue fluorescence, gotten ranging from 425 to 475 nm upon 405 nm excitation, corresponds to MitoView 405, marking mitochondrial site. The red fluorescence, recorded from 680 to 780 nm with 630 nm excitation, represents probe **B**, indicating the intracellular distribution of the probe. Scale bars are 50 μm.

efficiently targeted to mitochondria, supporting the proposed targeting mechanism based on electrostatic interactions. This strong correlation underscores the effectiveness of probe **B**'s mitochondrial targeting, suggesting it can reliably accumulate within the mitochondria of live cells without additional targeting groups. Such targeting is critical for studying mitochondrial dynamics and assessing changes related to mitochondrial function in real time. Given probe **B**'s high correlation with MitoView 405, it represents a promising tool for mitochondrial imaging applications, allowing researchers to track mitochondrial behavior and alterations under various conditions. This selective localization capability provides a robust foundation for exploring mitochondrial biology, including the investigation of dysfunctions and cellular stress responses in both physiological and pathological contexts.

Nystatin, an antifungal agent, disrupts cellular membrane integrity by binding to sterols, particularly ergosterol, within the cell membrane.[66,67] This interaction disturbs the normal fluidity of the lipid bilayer, leading to significant alterations in membrane dynamics and organization.[66,67] As nystatin integrates into the membrane, it increases the lipid bilayer's viscosity, resulting in a more viscous cellular environment. Furthermore, Nystatin-induced stress can trigger cellular responses that contribute to macromolecular aggregation and changes in the cytoskeleton, further elevating intracellular viscosity.[68] To investigate the effect of nystatin on cellular viscosity, we conducted experiments analogous to those

https://doi.org/10.1021/acsabm.4c01721
ACS Appl. Bio Mater. XXXX, XXX, XXX−XXX

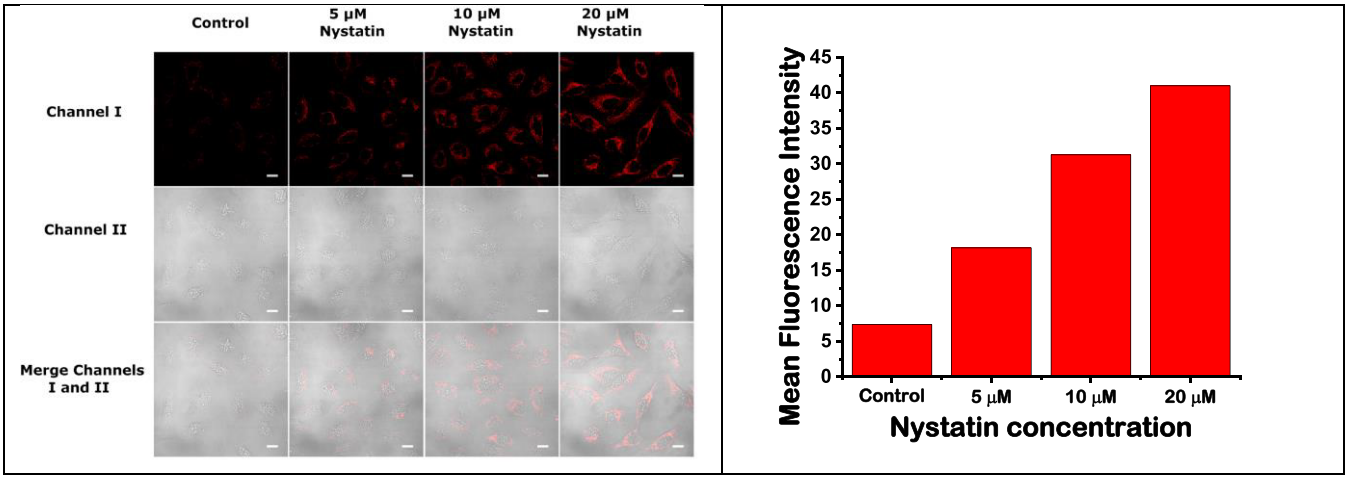

Figure 7. Fluorescence images of HeLa cells were exposed to increasing concentrations of Nystatin for 30 min, then, treated with probe **B** (5 μM) in DMEM for a further 20 min. Emission was detected within the 680−780 nm range using a 630 nm excitation wavelength. Scale bars indicate 50 μm.

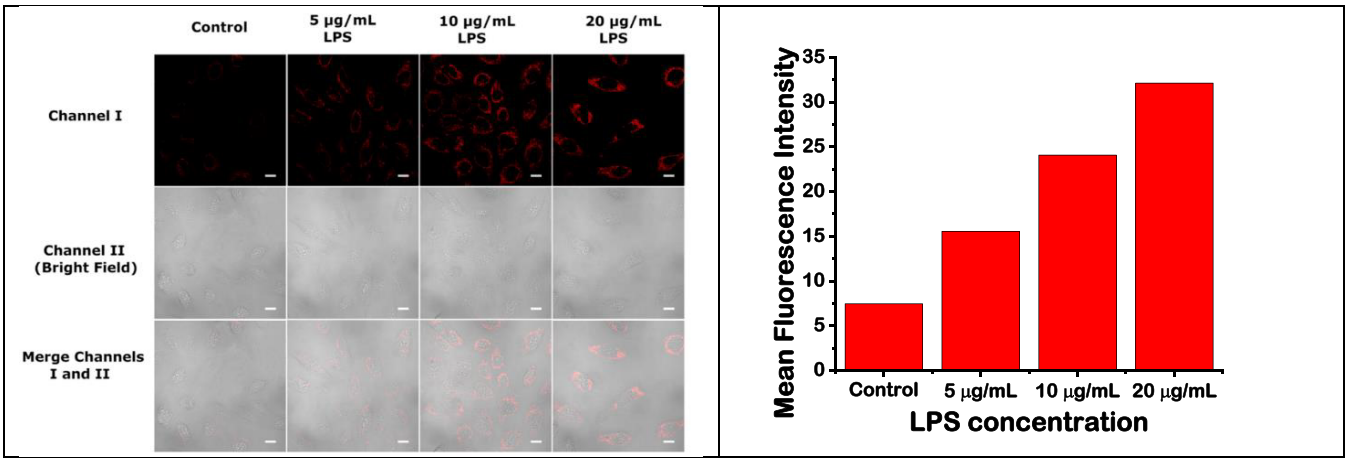

Figure 8. Fluorescence images showing HeLa cells exposed to different concentrations of LPS for 30 min, proceeding with a 20 min incubation with probe **B** (5 μM) in DMEM. Fluorescence was caught within the 680−780 nm range using a 630 nm excitation wavelength. Scale bars denote 50 μm.

performed with monensin. HeLa cells were treated with varying concentrations of nystatin for 30 min to induce changes in cellular viscosity. Following this treatment, cells were treated with probe **B** (5 μM) for 20 more minutes to allow for adequate probe uptake and fluorescence response (Figure 7). The fluorescence intensity of probe **B** was directly correlated with viscosity alterations. Our results demonstrated a progressive increase in fluorescence intensity corresponding to higher nystatin concentrations. In the control sample (0 μM nystatin), fluorescence was minimal, reflecting baseline cellular viscosity (Figure 7). Treatment with 5 μM nystatin led to a noticeable emission increase, indicating a moderate rise in viscosity. The fluorescence intensity further increased at 10 μM and peaked at 20 μM nystatin, showing a significant elevation in cellular viscosity (Figure 7). The enhanced fluorescence of probe **B** in response to Nystatin treatment reflects these viscosity changes. In summary, nystatin induces increases in cellular viscosity similar to monensin. These findings deliver essential insights into how agents like Nystatin influence cellular viscosity and highlight the potential of viscosity-sensitive probes for studying cellular responses to diverse compounds.

Bacterial-derived lipopolysaccharide (LPS) was employed to investigate its role in cellular viscosity changes in HeLa cells, serving as an alternative to nystatin. LPS, a vital element of the Gram-negative bacterial outer membrane,[69,70] is known to trigger potent immune responses and induce cellular stress through the activation of Toll-like receptor 4 (TLR4).[71,72] This activation leads to inflammatory pathways that affect various cellular processes, including membrane fluidity and intracellular viscosity. HeLa cells were exposed to different concentrations of LPS for 30 min to induce changes in cellular viscosity. Following this treatment, the cells were incubated with probe **B** (5 μM) for an extra 20 min to allow sufficient probe uptake and fluorescence response. The microscopy images revealed a marked increase in emission intensity correlating with higher concentrations of LPS (Figure 8). The control sample (0 μg/mL LPS) exhibited minimal fluorescence, indicating baseline cellular viscosity. A noticeable increase in fluorescence was observed at 5 μg/mL LPS, suggesting a moderate increase in viscosity. Fluorescence intensity continued to rise with increasing LPS concentrations, peaking at 20 μg/mL and indicating a substantial increase in cellular viscosity. The findings with LPS treatment were

https://doi.org/10.1021/acsabm.4c01721
ACS Appl. Bio Mater. XXXX, XXX, XXX−XXX

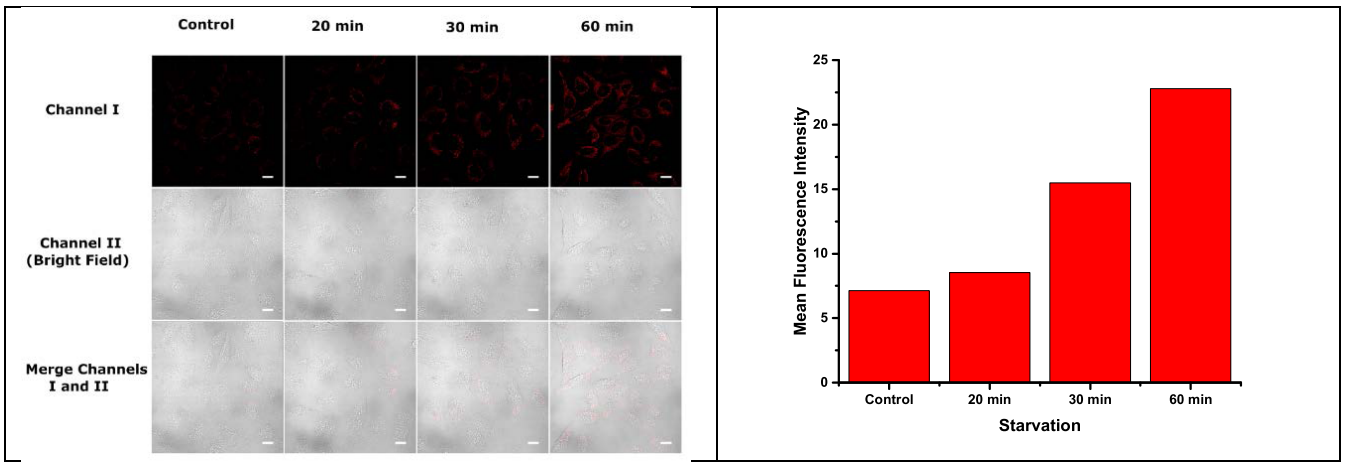

Figure 9. Time-course emission images of HeLa cells exposed to probe **B** (5 μM) in fetal bovine serum-free medium. Images were captured at different times post-treatment. Fluorescence emission was detected in the 680−780 nm range with excitation at 630 nm. Scale bars denote 50 μm.

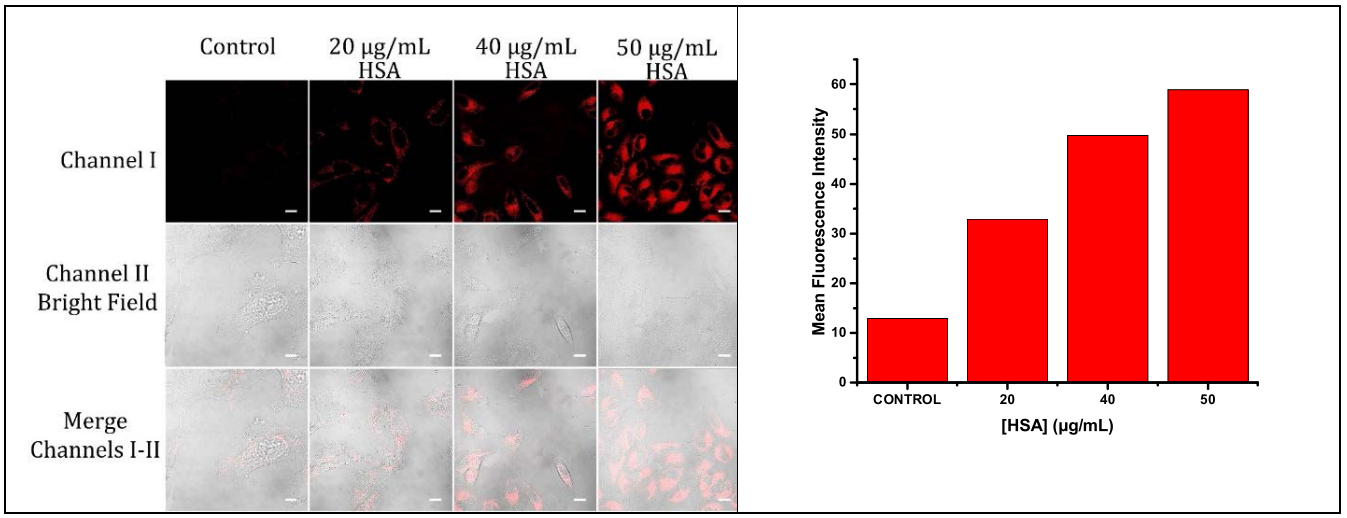

Figure 10. Emission images of HeLa cells exposed to varying HSA concentrations on HeLa cells for 30 min, proceeding with a further 30 min incubation with 10 μM probe **A**. Emission were gained within 700−800 nm range using a 633 nm excitation. Scale bars denote 50 μm.

consistent with those obtained using nystatin, confirming that LPS effectively increases cellular viscosity. LPS causes stress that affects membrane dynamics and the intracellular environment, leading to macromolecular aggregation and alterations in cytoskeletal structure, which in turn increase viscosity (Figure 8). Utilizing LPS in this experiment provided valuable insights into how inflammatory stimuli influences cellular viscosity. The consistent fluorescence responses across different viscosity-inducing agents, such as LPS and nystatin, validate the efficacy of probe **B** in detecting viscosity changes and underscore its utility for studying cellular responses to stress conditions. This approach enhances our understanding of viscosity's role in cellular processes under inflammatory and stress conditions.

To investigate how cellular starvation impacts viscosity,[25,73] HeLa cells were treated with probe **B** (5 μM) in fetal bovine serum-free medium. Time-course fluorescence microscopy was employed to observe changes in viscosity over different intervals. Images were captured at 0, 20, 40, and 60 min after the addition of probe **B**. Figure 9 presents fluorescence microscopy images showing an increase in fluorescence intensity of probe **B** over time. At 0 min, fluorescence intensity was relatively low, but it progressively increased at 20, 40, and 60 min. This gradual rise in fluorescence intensity indicates that cellular viscosity increases as starvation progresses. Cellular starvation triggers several stress responses, including mitophagy, which is the selective degradation of damaged or dysfunctional mitochondria.[74] As cells undergo mitophagy, there is an accumulation of cellular debris and alterations in the cellular environment, which can contribute to increased viscosity. Mitophagy often involves significant biochemical and structural changes within cells. As damaged mitochondria are processed and removed, the cellular environment can become more viscous due to the accumulation of waste products, reduced water content, and increased macromolecular aggregation. These changes can restrict molecular motion and enhance interactions with probe **B**, which is sensitive to viscosity variations. By tracking fluorescence intensity over time, we can infer the impact of starvation-induced cellular processes on viscosity (Figure 9). The results highlight probe **B**'s utility in studying cellular stress responses and provide insights into the relationship between mitophagy and viscosity changes, advancing our understanding of how cellular stress conditions affect cellular dynamics.

https://doi.org/10.1021/acsabm.4c01721
ACS Appl. Bio Mater. XXXX, XXX, XXX−XXX

To investigate the capability of probe **A** to detect human serum albumin (HSA) within a cellular environment, we assessed its fluorescence response in HeLa cells exposed to differing concentrations of HSA (20, 40, and 50 μg/mL). Following a 30 min treatment of HeLa cells with different HSA concentrations, the cells were treated with 10 μM probe **A** for a further 30 min (Figure 10). The results reveal a clear enhancement in cellular emission intensity with rising HSA concentrations (20, 40, and 50 μg/mL), demonstrating that probe **A**'s fluorescence is responsive to intracellular HSA levels. At 0 μg/mL HSA, used as the control, minimal fluorescence was observed, whereas incremental increases in HSA concentrations to 20, 40, and 50 μg/mL led to a corresponding enhancement in fluorescence intensity (Figure 10). This trend suggests a concentration-dependent interaction between probe **A** and HSA within the cellular environment. The observed fluorescence increase with higher HSA concentrations may be attributed to enhanced binding of probe **A** to HSA molecules within the cells. This interaction likely induces a conformational change in probe **A** that leads to fluorescence enhancement, making it sensitive to variations in HSA levels. The responsiveness of probe **A** to HSA within the physiological range indicates its potential as a valuable tool for monitoring HSA levels in live cells.

To explore the effects of monensin on viscosity within living organisms, fruit fly larvae were exposed to monensin at 20 μM and 40 μM levels for 4 h. After the monensin treatment, the larvae were then treated with 10 μM probe **B** for a further 2 h. For comparison, a control group was treated solely with 10 μM probe **B** for 2 h without monensin treatment. Figure 11 illustrates the confocal fluorescence microscopy images under these various conditions. The fluorescence intensity in the images increased with higher concentrations of monensin, showing progressively stronger fluorescence in flies treated with 20 and 40 μM monensin compared to the control group. The observed increase in fluorescence intensity in monensin-treated flies indicates a rise in viscosity within these specimens. The mechanism by which monensin affects cellular viscosity may involve several factors. Disruption of cellular ion balance and membrane integrity can induce cellular stress responses that alter the viscosity of the cellular environment. Additionally, monensin may cause the accumulation of cellular components or modifications in intracellular structures that contribute to increased viscosity. The results verify that probe **B** is greatly effective in detecting viscosity changes in vivo. The correlation between monensin level and fluorescence intensity demonstrates the probe's sensitivity to variations in viscosity, highlighting its utility as a tool for studying changes in cellular and tissue environments induced by chemical treatments (Figure 11). In summary, the increased fluorescence observed with higher monensin concentrations validates probe **B**'s capability to monitor viscosity changes in biological systems, offering valuable insights into how chemical treatments impact cellular and tissue properties.

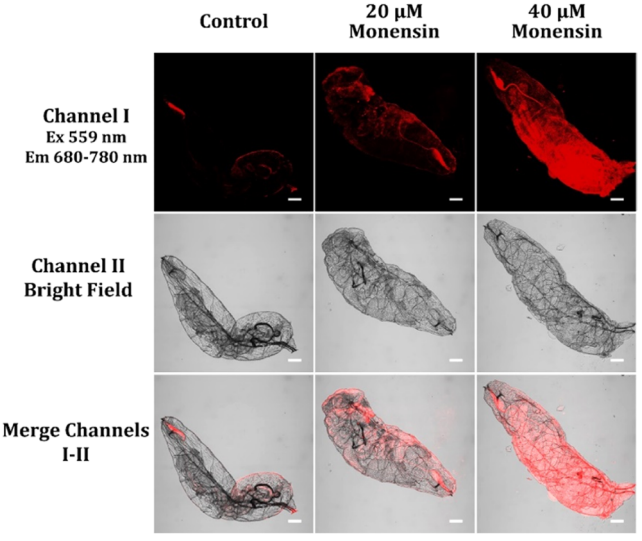

Figure 11. Fluorescence images of probe **B** in fruit flies under various treatment conditions. Fruit flies were treated with Monensin at concentrations of 20 and 40 μM for 4 h, incubated thereafter with 10 μM probe **B** for a further 2 h. As a control, fruit flies were given exposure to 10 μM probe **B** alone for 2 h without Monensin treatment. Fluorescence images were got in the 680−780 nm emission range using 630 nm excitation. Scale bar = 200 μm.

CONCLUSIONS

This research introduces an innovative approach to mitochondrial imaging with the development of two near-infrared (NIR) fluorescent probes, probes **A** and **B**, based on hemicyanine dyes integrated with rhodamine and 1,8-naphthalic derivatives. These probes exhibit optimized photophysical properties that allow for precise detection of mitochondrial viscosity, an essential marker for cellular health and function. The unique absorption and emission responses of the probes to varying viscosity levels underscore their sensitivity and versatility. Notably, probe **B** has shown exceptional performance in both cellular and in vivo contexts, accurately detecting and quantifying mitochondrial viscosity changes. This ability was validated through experiments with monensin, nystatin, and bacterial lipopolysaccharide (LPS), demonstrating the probe's robustness across diverse biological conditions. Additionally, probe **A** exhibited sensitivity to human serum albumin (HSA) levels, as demonstrated by its fluorescence enhancement in HeLa cells exposed to increasing concentrations of HSA. This result indicates the promise of probe **A** in real-time monitoring of HSA, a crucial biomarker for liver and kidney health, in live cellular systems. Overall, the high selectivity, photostability, and low cytotoxicity of probe **B** make it a valuable tool for exploring mitochondrial function and stress responses, while probe **A**'s sensitivity to HSA expands its utility in monitoring essential biomolecules in live cells. These findings not only advance our understanding of mitochondrial and cellular dynamics but also open new avenues for research into mitochondrial-related and albumin-associated diseases, underscoring the potential of NIR fluorescent probes in both basic and applied biomedical research.

ASSOCIATED CONTENT

Supporting Information

The Supporting Information is available free of charge at https://pubs.acs.org/doi/10.1021/acsabm.4c01721.

Comprehensive overview of the instrumentation and reagents used; synthesis of probes **A** and **B** and their corresponding precursors; NMR and MS spectra for both the intermediates and the final probes; fluorescence data for the probes are presented, measured at different concentrations of glycerol and HSA; assessments of their photostability and selectivity; experimental procedures

https://doi.org/10.1021/acsabm.4c01721
ACS Appl. Bio Mater. XXXX, XXX, XXX−XXX

for culturing HeLa cells and imaging *Drosophila melanogaster* larvae; evaluate the probes' effectiveness in biological systems; cell viability results from the MTT assay following probe treatment are also included; supported by theoretical calculations that align with the experimental observations and molecular docking (PDF)

AUTHOR INFORMATION

Corresponding Authors

Sushil K. Dwivedi − *Department of Chemistry, Michigan Technological University, Houghton, Michigan 49931, United States; Health Research Institute, Michigan Technological University, Houghton, Michigan 49931, United States;* orcid.org/0000-0003-2744-9521; Email: sdwive2@mtu.edu

Athar Ata − *Department of Chemistry, Michigan Technological University, Houghton, Michigan 49931, United States;* Email: aata@mtu.edu

Rudy Lin Luck − *Department of Chemistry, Michigan Technological University, Houghton, Michigan 49931, United States;* orcid.org/0000-0001-5436-1942; Email: rluck@mtu.edu

Haiying Liu − *Department of Chemistry, Michigan Technological University, Houghton, Michigan 49931, United States; Health Research Institute, Michigan Technological University, Houghton, Michigan 49931, United States;* orcid.org/0000-0001-8351-2017; Email: hyliu@mtu.edu

Authors

Adenike Mary Olowolagba − *Department of Chemistry, Michigan Technological University, Houghton, Michigan 49931, United States; Health Research Institute, Michigan Technological University, Houghton, Michigan 49931, United States*

Omowunmi Rebecca Aworinde − *Department of Chemistry, Michigan Technological University, Houghton, Michigan 49931, United States; Health Research Institute, Michigan Technological University, Houghton, Michigan 49931, United States*

Micah Olamide Idowu − *Department of Chemistry, Michigan Technological University, Houghton, Michigan 49931, United States*

Dilka Liyana Arachchige − *Department of Chemistry, Michigan Technological University, Houghton, Michigan 49931, United States; Health Research Institute, Michigan Technological University, Houghton, Michigan 49931, United States*

Crystal Wang − *Houghton High School, Houghton, Michigan 49931, United States*

Olivya Rose Graham − *Health Research Institute and Department of Biological Sciences, Michigan Technological University, Houghton, Michigan 49931, United States*

Joseph Peters − *Department of Chemistry, Michigan Technological University, Houghton, Michigan 49931, United States; Health Research Institute, Michigan Technological University, Houghton, Michigan 49931, United States*

Grace Rickauer − *Department of Chemistry, Michigan Technological University, Houghton, Michigan 49931, United States; Health Research Institute, Michigan Technological University, Houghton, Michigan 49931, United States*

Thomas Werner − *Health Research Institute and Department of Biological Sciences, Michigan Technological University, Houghton, Michigan 49931, United States*

Complete contact information is available at: https://pubs.acs.org/10.1021/acsabm.4c01721

Author Contributions

A.M.O., O.R.A., and S.K.D.: Investigation, methodology, data curation, and formal analysis. S.K.D.: Supervised graduate and undergraduate students. M.O.I., D.L.A., C.W., and J.P.: Contributed to validation. O.R.G.: Data curation. R.L.: Specialized in computational chemistry. T.W. and A.A.: Provided supervision and manuscript editing. H.L.: Funding acquisition, project administration, conceptualization, and manuscript preparation and editing. All authors have approved the final version of the manuscript.

Notes

The authors declare no competing financial interest.

ACKNOWLEDGMENTS

The National Institute of General Medical Sciences, part of the National Institutes of Health, funded our work through award numbers 2R15GM114751 and R15GM114751, both awarded to H. Liu, and R15GM146206-01, awarded to H. Liu and R.L. Luck. The support from these organizations was instrumental in the success of this study, and we are grateful for their contributions to advancing research and scientific knowledge in this field. We also wish to express our sincere appreciation to the National Science Foundation for their financial support through award number 2117318. The funding enabled the purchase of a new NMR spectrometer, which was essential for characterizing the chemical structures of the fluorescent probes. H. Liu was the recipient of this grant.

REFERENCES

(1) Fan, T. J.; Xia, L.; Han, Y. R. Mitochondrion and apoptosis. *Acta Biochim. Biophys. Sin.* **2001**, *33* (1), 7−12.

(2) Jardim, F. R.; de Rossi, F. T.; Nascimento, M. X.; Barros, R. G. D.; Borges, P. A.; Prescilio, I. C.; de Oliveira, M. R. Resveratrol and Brain Mitochondria: a Review. *Mol. Neurobiol.* **2018**, *55* (3), 2085−2101.

(3) Lloreta-Trull, J.; Serrano, S. Biology and pathology of the mitochondrion. *Ultrastruct. Pathol.* **1998**, *22* (5), 357−367.

(4) Maurya, S. K.; Gupta, S.; Bakshi, A.; Kaur, H.; Jain, A.; Senapati, S.; Baghel, M. S. Targeting mitochondria in the regulation of neurodegenerative diseases: A comprehensive review. *J. Neurosci. Res.* **2022**, *100* (10), 1845−1861.

(5) Picard, M.; McEwen, B. S. Psychological Stress and Mitochondria: A Systematic Review. *Psychosom. Med.* **2018**, *80* (2), 141−153.

(6) Jung, Y. L.; Yang, Y. J.; Shil, A.; Sarkar, S.; Ahn, K. H. Anticancer Prodrug Capable of Mitochondria-Targeting, Light-Triggered Release, and Fluorescence Monitoring. *ACS Appl. Bio Mater.* **2024**, *7* (6), 3991−3996.

(7) Li, H. D.; Kim, H.; Zhang, C.; Zeng, S.; Chen, Q. X.; Jia, L. Y.; Wang, J. Y.; Peng, X. J.; Yoon, J. Mitochondria-targeted smart AIEgens: Imaging and therapeutics. *Coord. Chem. Rev.* **2022**, *473*, No. 214818.

(8) Arachchige, D. L.; Dwivedi, S. K.; Jaeger, S.; Olowolagba, A. M.; Mahmoud, M.; Tucker, D. R.; Fritz, D. R.; Werner, T.; Tanasova, M.; Luck, R. L.; Liu, H. Highly Sensitive Cyanine Dyes for Rapid Sensing of NAD(P)H in Mitochondria and First-Instar Larvae of *Drosophila melanogaster*. *ACS Appl. Bio Mater.* **2023**, *6* (8), 3199−3212.

(9) Li, Z. Q.; Chen, M. L.; Zhu, W. K.; Xin, R. Q.; Yang, J. H.; Hu, S. Y.; You, J. M.; Ryu, D.; Lim, S. H.; Li, S.; Kim, J. Advances and perspectives of composite nanoarchitectonics of nanocellulose/metal-organic frameworks for effective removal of volatile organic compounds. *Coord. Chem. Rev.* **2024**, *520*, No. 216142.
(10) Huang, Y. F.; Liang, J. P.; Fan, Z. F. A review: Small organic molecule dual/multi-organelle-targeted fluorescent probes. *Talanta* **2023**, *259*, No. 124529.
(11) Lee, S. C.; Heo, J.; Woo, H. C.; Lee, J. A.; Seo, Y. H.; Lee, C. L.; Kim, S.; Kwon, O. P. Fluorescent Molecular Rotors for Viscosity Sensors. *Chem. - Eur. J.* **2018**, *24* (52), 13706−13718.
(12) Ma, C. G.; Sun, W.; Xu, L. M.; Qian, Y.; Dai, J. A.; Zhong, G. Y.; Hou, Y.; Liu, J. L.; Shen, B. X. A minireview of viscosity-sensitive fluorescent probes: design and biological applications. *J. Mater. Chem. B* **2020**, *8* (42), 9642−9651.
(13) Miao, W.; Yu, C. J.; Hao, E. H.; Jiao, L. J. Functionalized BODIPYs as Fluorescent Molecular Rotors for Viscosity Detection. *Front. Chem.* **2019**, *7*, No. 825, DOI: 10.3389/fchem.2019.00825.
(14) Pareek, N.; Mendiratta, S.; Kalita, N.; Sivaramakrishnan, S.; Khan, R. S.; Samanta, A. Unraveling Ferroptosis Mechanisms: Tracking Cellular Viscosity with Small Molecular Fluorescent Probes. *Chem. - Asian J.* **2024**, *19* (8), No. e202400056, DOI: 10.1002/asia.202400056.
(15) Xiao, H. B.; Li, P.; Tang, B. Small Molecular Fluorescent Probes for Imaging of Viscosity in Living Biosystems. *Chem. - Eur. J.* **2021**, *27* (23), 6880−6898.
(16) Yang, X. P.; Zhang, D.; Ye, Y.; Zhao, Y. F. Recent advances in multifunctional fluorescent probes for viscosity and analytes. *Coord. Chem. Rev.* **2022**, *453*, No. 214336.
(17) Khan, Z.; Sekar, N. Deep Red to NIR Emitting Xanthene Hybrids: Xanthene-Hemicyanine Hybrids and Xanthene-Coumarin Hybrids. *ChemistrySelect* **2023**, *8* (5), No. e202203377, DOI: 10.1002/slct.202203377.
(18) Luo, P.; Wang, M.; Liu, W. G.; Liu, L.; Xu, P. Activity-Based Fluorescent Probes Based on Hemicyanine for Biomedical Sensing. *Molecules* **2022**, *27* (22), No. 7750.
(19) Zeng, Z. L.; Liew, S. S.; Wei, X.; Pu, K. Y. Hemicyanine-Based Near-Infrared Activatable Probes for Imaging and Diagnosis of Diseases. *Angew. Chem., Int. Ed.* **2021**, *60* (51), 26454−26475.
(20) Lei, Y. J.; Wu, X. S.; Yao, Q. J. A New Hemicyanine-based Fluorophore for Monitoring pH and Lysosome Imaging. *J. Anal. Chem.* **2019**, *74* (9), 940−944.
(21) Mazi, W.; Adhikari, R.; Zhang, Y. B.; Xia, S.; Fang, M. X.; Luck, R. L.; Tajiri, M.; Tiwari, A.; Tanasova, M.; Liu, H. Y. Fluorescent probes with high pKa values based on traditional, near-infrared rhodamine, and hemicyanine fluorophores for sensitive detection of lysosomal pH variations. *Methods* **2019**, *168*, 40−50.
(22) Mazi, W.; Yan, Y. N.; Zhang, Y. B.; Xia, S.; Wan, S. L.; Tajiri, M.; Luck, R. L.; Liu, H. Y. A near-infrared fluorescent probe based on a hemicyanine dye with an oxazolidine switch for mitochondrial pH detection. *J. Mater. Chem. B* **2021**, *9* (3), 857−863.
(23) Miao, J. T.; Fan, C.; Shi, X. Y.; Sun, R.; Xu, Y. J.; Ge, J. F. Colorimetric and ratiometric pH responses by the protonation of phenolate within hemicyanine. *Analyst* **2014**, *139* (23), 6290−6297.
(24) Xia, S.; Wang, J. B.; Bi, J. H.; Wang, X.; Fang, M. X.; Phillips, T.; May, A.; Conner, N.; Tanasova, M.; Luo, F. T.; Liu, H. Fluorescent probes based on π-conjugation modulation between hemicyanine and coumarin moieties for ratiometric detection of pH changes in live cells with visible and near-infrared channels. *Sens. Actuators, B* **2018**, *265*, 699−708.
(25) Xia, S. A.; Wang, J. B.; Zhang, Y. B.; Whisman, N.; Bi, J. H.; Steenwinkel, T. E.; Wan, S. L.; Medford, J.; Tajiri, M.; Luck, R. L.; et al. Ratiometric fluorescent probes based on through-bond energy transfer of cyanine donors to near-infrared hemicyanine acceptors for mitochondrial pH detection and monitoring of mitophagy. *J. Mater. Chem. B* **2020**, *8* (8), 1603−1615.
(26) Yan, Y. N.; Zhang, Y. B.; Xia, S.; Wan, S. L.; Vohs, T.; Tanasova, M.; Luck, R. L.; Liu, H. Y. Ratiometric Near-Infrared Fluorescent Probes Based on Hemicyanine Dyes Bearing Dithioacetal and Formal Residues for pH Detection in Mitochondria. *Molecules* **2021**, *26* (7), No. 2088.
(27) Gong, J.; Liu, C.; Jiao, X. J.; He, S.; Zhao, L. C.; Zeng, X. S. Novel mitochondria-targeted viscosity probe based on a fluorescent rotatable xanthene-hemicyanine dyad. *Microchem. J.* **2020**, *158*, No. 105191.
(28) Liu, H. J.; Zhu, M. S.; Zhang, G.; Sun, R.; Xu, Y. J.; Ge, J. F. Viscosity probes towards different organelles with red emission based on an identical hemicyanine structure. *Analyst* **2023**, *148* (18), 4463−4469.
(29) Wang, Y. N.; Xu, B.; Qiu, L. H.; Sun, R.; Xu, Y. J.; Ge, J. F. Viscosity sensitive fluorescent dyes with excellent photostability based on hemicyanine dyes for targeting cell membrane. *Sens. Actuators, B* **2021**, *337*, No. 129787.
(30) Wei, Y. F.; Weng, X. F.; Sha, X. L.; Sun, R.; Xu, Y. J.; Ge, J. F. Simultaneous imaging of lysosomal and mitochondrial viscosity under different conditions using a NIR probe. *Sens. Actuators, B* **2021**, *326*, No. 128954.
(31) Xu, S. L.; Guo, F. F.; Xu, Z. H.; Wang, Y.; James, T. D. A hemicyanine-based fluorescent probe for ratiometric detection of ClO-and turn-on detection of viscosity and its imaging application in mitochondria of living cells and zebrafish. *Sens. Actuators, B* **2023**, *383*, No. 133510.
(32) Yang, X. Z.; Xu, B.; Shen, L.; Sun, R.; Xu, Y. J.; Song, Y. L.; Ge, J. F. Series of Mitochondria/Lysosomes Self-Targetable Near-Infrared Hemicyanine Dyes for Viscosity Detection. *Anal. Chem.* **2020**, *92* (5), 3517−3521.
(33) Zeng, S.; Wang, Y.; Chen, C.; Kim, H.; Liu, X. S.; Jiang, M. J.; Yu, Y. C.; Kafuti, Y. S.; Chen, Q. X.; Wang, J. Y.; et al. An ER-targeted, Viscosity-sensitive Hemicyanine Dye for the Diagnosis of Non-alcoholic Fatty Liver and Photodynamic Cancer Therapy by Activating Pyroptosis Pathway. *Angew. Chem., Int. Ed.* **2024**, *63* (9), No. e202316487, DOI: 10.1002/anie.202316487.
(34) Zhang, X. F.; Ma, X. Y.; Zhang, B. Y.; Yang, D. W.; Bai, R. Y.; Gao, Y. X.; Sun, H. X.; Tang, Y. L.; Shi, L. Design and Screening of Fluorescent Probes Based upon Hemicyanine Dyes for Monitoring Mitochondrial Viscosity in Living Cells. *J. Phys. Chem. B* **2024**, *128* (16), 3910−3918.
(35) Li, H. D.; Kim, H.; Xu, F.; Han, J. J.; Yao, Q. C.; Wang, J. Y.; Pu, K. Y.; Peng, X. J.; Yoon, J. Activity-based NIR fluorescent probes based on the versatile hemicyanine scaffold: design strategy, biomedical applications, and outlook. *Chem. Soc. Rev.* **2022**, *51* (5), 1795−1835.
(36) Pakrashy, S.; Chakraborty, S.; Manna, S.; Goswami, J. N.; Bhattacharya, B.; Emmerling, F.; Mandal, J.; Misra, S.; Choudhury, S. M.; Okla, M. K.; et al. Inhibition of Human Colorectal Cancer by a Natural Product 7-Acetylhorminone and Interactions with BSA/HSA: Multispectral Analysis and In Silico and In Vitro Studies. *ACS Appl. Bio Mater.* **2024**, *7* (5), 3414−3430.
(37) Chao, J. J.; Zhang, H.; Wang, Z. Q.; Liu, Q. R.; Mao, G. J.; Chen, D. H.; Li, C. Y. A near-infrared fluorescent probe for monitoring abnormal mitochondrial viscosity in cancer and fatty-liver mice model. *Anal. Chim. Acta* **2023**, *1242*, No. 340813.
(38) Chao, J. J.; Zhang, H.; Wang, Z. Q.; Liu, Q. R.; Mao, G. J.; Li, Y. F.; Li, C. Y. A near-infrared fluorescent probe for viscosity: Differentiating cancer cells from normal cells and dual-modal imaging in tumor mice. *Anal. Chim. Acta* **2024**, *1285*, No. 342024.
(39) Chen, B. C.; Mao, S. M.; Sun, Y. Y.; Sun, L. Y.; Ding, N.; Li, C. D.; Zhou, J. A mitochondria-targeted near-infrared fluorescent probe for imaging viscosity in living cells and a diabetic mice model. *Chem. Commun.* **2021**, *57* (36), 4376−4379.
(40) Liao, Q. T.; Chao, J. J.; Wang, W. X.; Liu, T.; Mao, G. J.; Xu, F.; Li, C. Y. A novel near-infrared fluorescent probe for the imaging of viscosity in cells and tumor-bearing mice. *Chem. Commun.* **2023**, *59* (37), 5607−5610.
(41) Ma, Y. Y.; Zhao, Y. P.; Guo, R.; Zhu, L. L.; Lin, W. Y. A near-infrared emission fluorescent probe with multi-rotatable moieties for highly sensitive detection of mitochondrial viscosity in an inflammatory cell model. *J. Mater. Chem. B* **2018**, *6* (39), 6212−6216.

https://doi.org/10.1021/acsabm.4c01721
ACS Appl. Bio Mater. XXXX, XXX, XXX−XXX

(42) Shi, W. J.; Wei, Y. F.; Yang, J. R.; Li, H. Z.; Wan, Q. H.; Wang, Y. X.; Leng, H. X.; Chen, K.; Yan, J. W. Novel meso-trifluoromethyl BODIPY-based near-infrared-emitting fluorescent probes for organelle-specific imaging of cellular viscosity. *Sens. Actuators, B* **2022**, *359*, No. 131594.
(43) Wang, H. L.; Zheng, H. Y.; Zhang, W. J.; Yang, L.; Yu, M. M.; Li, Z. X. A near-infrared aggregation-induced emission probe for imaging lipid droplet and in vivo visualization of diabetes-related viscosity variations. *Sens. Actuators, B* **2023**, *394*, No. 134347.
(44) Wang, P. P.; Ai, S. W.; Deng, M.; Liu, Y.; Liu, Y.; He, L. W.; Li, S. J. A lysosomal-targeted and viscosity-ultrasensitive near-infrared fluorescent probe for sensing viscosity in cells and a diabetic mice model. *Talanta* **2024**, *278*, No. 126506.
(45) Wu, X.; Zhang, R. X.; Li, Y.; Gai, Y. T.; Feng, T. T.; Kou, J. J.; Kong, F. P.; Li, L.; Tang, B. Rational Design of MMP-Independent Near-Infrared Fluorescent Probes for Accurately Monitoring Mitochondrial Viscosity. *Anal. Chem.* **2023**, *95* (19), 7611−7619.
(46) Zheng, A. S.; Liu, H.; Gao, X. N.; Xu, K. H.; Tang, B. A Mitochondrial-Targeting Near-Infrared Fluorescent Probe for Revealing the Effects of Hydrogen Peroxide And Heavy Metal Ions on Viscosity. *Anal. Chem.* **2021**, *93* (26), 9244−9249.
(47) Dong, B. L.; Song, W. H.; Lu, Y. R.; Sun, Y. R.; Lin, W. Y. Revealing the Viscosity Changes in Lipid Droplets during Ferroptosis by the Real-Time and In Situ Near-Infrared Imaging. *ACS Sens.* **2021**, *6* (1), 22−26.
(48) Hong, J. X.; Guan, X. G.; Chen, Y.; Tan, X. D.; Zhang, S. Y.; Feng, G. Q. Mitochondrial Membrane Potential Independent Near-Infrared Mitochondrial Viscosity Probes for Real-Time Tracking Mitophagy. *Anal. Chem.* **2023**, *95* (13), 5687−5694.
(49) Wu, X.; Wang, X. X.; Li, Y.; Kong, F. P.; Xu, K. H.; Li, L.; Tang, B. A Near-Infrared Probe for Specific Imaging of Lipid Droplets in Living Cells. *Anal. Chem.* **2022**, *94* (11), 4881−4888.
(50) Yin, J. L.; Kong, X. Q.; Lin, W. Y. Noninvasive Cancer Diagnosis In Vivo Based on a Viscosity-Activated Near-Infrared Fluorescent Probe. *Anal. Chem.* **2021**, *93* (4), 2072−2081.
(51) Zhang, Y. Y.; Li, Z.; Hu, W.; Liu, Z. H. A Mitochondrial-Targeting Near-Infrared Fluorescent Probe for Visualizing and Monitoring Viscosity in Live Cells and Tissuese. *Anal. Chem.* **2019**, *91* (15), 10302−10309.
(52) Ma, X.; Sun, R.; Cheng, J.; Liu, J.; Gou, F.; Xiang, H.; Zhou, X. Fluorescence aggregation-caused quenching versus aggregation-induced emission: a visual teaching technology for undergraduate chemistry students. *J. Chem. Educ.* **2016**, *93* (2), 345−350.
(53) Dwivedi, S. K.; Arachchige, D. L.; Vohs, T.; Tang, J.; Usimaki, K.; Olowolagba, A. M.; Fritz, D. R.; Luck, R. L.; Werner, T.; Liu, H. Near-infrared rhodol dyes bearing salicylaldehyde moieties for ratiometric pH sensing in live cells during mitophagy and under hypoxia conditions. *J. Mater. Chem. B* **2023**, *11* (13), 2852−2861.
(54) Arachchige, D. L.; Dwivedi, S. K.; Olowolagba, A. M.; Peters, J.; Beatty, A. C.; Guo, A.; Wang, C.; Werner, T.; Luck, R. L.; Liu, H. Y. Dynamic insights into mitochondrial function: Monitoring viscosity and SO_2 levels in living cells. *J. Photochem. Photobiol., B* **2024**, *258*, No. 112986.
(55) Fang, M. X.; Adhikari, R.; Bi, J. H.; Mazi, W.; Dorh, N.; Wang, J. B.; Conner, N.; Ainsley, J.; Karabencheva-Christova, T. G.; Luo, F. T.; et al. Fluorescent probes for sensitive and selective detection of pH changes in live cells in visible and near-infrared channels. *J. Mater. Chem. B* **2017**, *5* (48), 9579−9590.
(56) Wan, S. L.; Xia, S.; Medford, J.; Durocher, E.; Steenwinkel, T. E.; Rule, L.; Zhang, Y. B.; Luck, R. L.; Werner, T.; Liu, H. Y. A ratiometric near-infrared fluorescent probe based on a novel reactive cyanine platform for mitochondrial pH detection. *J. Mater. Chem. B* **2021**, *9* (25), 5150−5161.
(57) Xia, S.; Fang, M. X.; Wang, J. B.; Bi, J. H.; Mazi, W.; Zhang, Y. B.; Luck, R. L.; Liu, H. Y. Near-infrared fluorescent probes with BODIPY donors and rhodamine and merocyanine acceptors for ratiometric determination of lysosomal pH variance. *Sens. Actuators, B* **2019**, *294*, 1−13.
(58) Zhang, Y. B.; Arachchige, D. L.; Olowolagba, A.; Luck, R. L.; Liu, H. Y. Near-infrared fluorescent probe based on rhodamine derivative for detection of NADH in live cells. *Methods* **2022**, *204*, 22−28.
(59) Arachchige, D. L.; Dwivedi, S. K.; Waters, M.; Jaeger, S.; Peters, J.; Tucker, D. R.; Geborkoff, M.; Werner, T.; Luck, R. L.; Godugu, B.; Liu, H. Sensitive monitoring of NAD(P)H levels within cancer cells using mitochondria-targeted near-infrared cyanine dyes with optimized electron-withdrawing acceptors. *J. Mater. Chem. B* **2024**, *12* (2), 448−465.
(60) Dwivedi, S. K.; Arachchige, D. L.; Olowolagba, A.; Mahmoud, M.; Cunnien, J.; Tucker, D. R.; Fritz, D.; Werner, T.; Luck, R. L.; Liu, H. Y. Thiophene-based organic dye with large Stokes shift and deep red emission for live cell NAD(P)H detection under varying chemical stimuli. *J. Mater. Chem. B* **2023**, *11* (27), 6296−6307.
(61) Dwivedi, S. K.; Arachchige, D. L.; Waters, M.; Jaeger, S.; Mahmoud, M.; Olowolagba, A. M.; Tucker, D. R.; Geborkoff, M. R.; Werner, T.; Luck, R. L.; et al. Near-infrared absorption and emission probes with optimal connection bridges for live monitoring of NAD(P)H dynamics in living systems. *Sens. Actuators, B* **2024**, *402*, No. 135073.
(62) Norouzi, M.; Amoli, A.; Zhang, Y.; Zhang, Y.; Beatty, A. C.; Jarvi, A.; Ata, A.; Werner, T.; Liu, H. Y. Deep-Red and Near-Infrared Compact Cyanine Dyes for Sensitive NAD(P)H Sensing in Live Cells and Kidney Disease Tissues. *ACS Appl. Bio Mater.* **2024**, *7*, 8552−8564.
(63) Jaeger, S.; Lanquaye, H.; Dwivedi, S. K.; Arachchige, D. L.; Xia, J. M.; Waters, M.; Bigari, B. L.; Olowolagba, A. M.; Agyemang, P.; Zhang, Y.; et al. Near-Infrared Visualization of NAD(P)H Dynamics in Live Cells and *Drosophila melanogaster* Larvae Using a Coumarin-Based Pyridinium Fluorescent Probe. *ACS Appl. Bio Mater.* **2024**, *7*, 8465.
(64) Rajendran, V.; Ilamathi, H. S.; Dutt, S.; Lakshminarayana, T. S.; Ghoshi, P. C. Chemotherapeutic Potential of Monensin as an Antimicrobial Agent. *Curr. Top. Med. Chem.* **2019**, *18* (22), 1976−1986.
(65) Chen, Q.; Zhang, X. F.; Wang, T.; Cao, X. Q.; Shen, S. L. A sensitive NIR mitochondria-targeting fluorescence probe for visualizing viscosity in living cells and mice. *Anal. Chim. Acta* **2022**, *1231*, No. 340443.
(66) Lyu, X.; Zhao, C.; Yan, Z. M.; Hua, H. Efficacy of nystatin for the treatment of oral candidiasis: a systematic review and meta-analysis. *Drug Des., Dev. Ther.* **2016**, *10*, 1161−1171.
(67) Schäfer-Korting, M.; Blechschmidt, J.; Korting, H. C. Clinical use of oral nystatin in the prevention of systemic candidosis in patients at particular risk. *Mycoses* **1996**, *39* (9−10), 329−339.
(68) Pan, X. H.; Wang, C.; Zhao, C. C.; Cheng, T. T.; Zheng, A. S.; Cao, Y. R.; Xu, K. H. Assessment of cancer cell migration using a viscosity-sensitive fluorescent probe. *Chem. Commun.* **2022**, *58* (29), 4663−4666.
(69) Caroff, M.; Karibian, D. Structure of bacterial lipopolysaccharides. *Carbohydr. Res.* **2003**, *338* (23), 2431−2447.
(70) Penagonda, V.; Hilton, A. C.; Chen, G. Impact of Lipopolysaccharide Extraction on Bacterial Adhesion and Transport. *J. Adhes. Sci. Technol.* **2008**, *22* (10−11), 1073−1088.
(71) Knapp, S.; Wieland, C. W.; Florquin, S.; Pantophlet, R.; Dijkshoorn, L.; Tshimbalanga, N.; Akira, S.; van der Poll, T. Differential roles of CD14 and Toll-like receptors 4 and 2 in murine *Acinetobacter* pneumonia. *Am. J. Respir. Crit. Care Med.* **2006**, *173* (1), 122−129.
(72) Smith, N. J.; Varley, C. L.; Eardley, I.; Feather, S.; Trejdosiewicz, L. K.; Southgate, J. Toll-Like Receptor Responses of Normal Human Urothelial Cells to Bacterial Flagellin and Lipopolysaccharide. *J. Urol.* **2011**, *186* (3), 1084−1092.
(73) Dwivedi, S. K.; Arachchige, D. L.; Vohs, T.; Tang, J. N.; Usimaki, K.; Olowolagba, A. M.; Fritz, D. R.; Luck, R. L.; Werner, T.; Liu, H. Y. Near-infrared rhodol dyes bearing salicylaldehyde moieties for ratiometric pH sensing in live cells during mitophagy and under hypoxia conditions. *J. Mater. Chem. B* **2023**, *11* (13), 2852−2861.

https://doi.org/10.1021/acsabm.4c01721
ACS Appl. Bio Mater. XXXX, XXX, XXX−XXX

(74) Mukhopadhyay, S.; Naik, P. P.; Panda, P. K.; Sinha, N.; Das, D. N.; Bhutia, S. K. Serum starvation induces anti-apoptotic cIAP1 to promote mitophagy through ubiquitination. *Biochem. Biophys. Res. Commun.* **2016**, *479* (4), 940−946.

https://doi.org/10.1021/acsabm.4c01721
ACS Appl. Bio Mater. XXXX, XXX, XXX−XXX